25th ABCM International Congress of Mechanical Engineering
October 20-25, 2019, Uberlândia, MG, Brazil

# COB-2019-0748
# NUMERICAL SOLUTION USING SPH METHOD: AN APPLICATION TO TRANSIENT HEAT CONDUCTION

**Almério José Venâncio Pains Soares Pamplona**
**Karoliny Freitas Silva**
**Claúdio Lustosa Bucar Filho**
**Joel Roberto Guimarães Vasco**
Universidade Federal de Goiás - Av. Universitária, 1488, Qd. 86, Bloco A, Setor Leste Universitário, Goiânia, Goiás, 74605-010
almeriopamplona@gmail.com
karolinyecristo@gmail.com
claudiolbfilho@gmail.com
joelvasco@ufg.br

***Abstract.*** *The unsteady-state heat conduction on a rectangular plate is analyzed assuming the Dirichlet boundary condition and properties linear behavior such that the superposition hypothesis can be applied. Under these conditions, it is used the Fourier analysis method to find an analytical solution, which is a triple infinite series of sinusoidal functions and an exponential time decreasing function. This solution is used as a reference to further comparisons for two numerical methods used in the present paper. The first mentioned numerical technique is the Smoothed Particle Hydrodynamics method (SPH), which uses particles to model the physical domain of the study object and a kernel function to interpolate the properties of the particles such as temperature, velocity, and density. As a result, there is no need for a numerical mesh, allowing complex geometries modeling. The second technique is the Finite Differential Method (FDM), which has a discrete numerical mesh of the physical domain and a finite difference approach to discretize the governing equations. Both methods are applied to the unsteady-state heat conduction problem, resulting in isothermal curves evolving through the time until they reach the steady-state. Comparing them with the analytical solution, it is found a similar accuracy of order* $10^{-2}$*, although the SPH method has a higher computational cost. Moreover, it is studied the behavior of the particle mass definition equation for SPH under the influence of the smoothed length and the material properties.*

***Keywords:****Transient Heat Conduction, SPH, FDM*

## 1. INTRODUCTION

The heat transfer is present in various engineering applications. One of them is the effects of transient heat flow in engine design caused by the internal combustion of its combustion chamber (Mavropoulos, 2011). Safety in mine hoisting can be evaluated through the heat conduction on wire rope caused by its friction with the fixed lining outside the drum (Peng et al., 2011). Moreover, new mathematical models to study those engineering applications have been proposed, such as the model for transient convectively processes on the heated surfaces of a boiler proposed by Zima (2011).

These mathematical models can have analytical solutions for some simple geometries and boundary conditions or, at least, analyzed by some mathematical tools (Myint-U and Debnath, 2007). However, various engineering applications are ill-posed (Beck et al., 1985; Tanana and Sidikova, 2018) or hard to be analytically solved, such as unsteady-state problems at composite slabs (Deconinck et al., 2014; Chiba, 2018) or with non-classical initial and boundary condition (Ceretani et al., 2015; Kudinov et al., 2015). Therefore, numerical techniques are a practical approach to overcome the mathematical analysis limitations.

A numerical method used to solve a complex problem is the Smoothed Particle Hydrodynamics (SPH). It is a meshfree, particle-based and Lagrangian numerical method, originally developed to solve astrophysical phenomena (Gingold and Monaghan, 1977; Lucy, 1977). As a particle-based method, it uses a kernel function to smoothly interpolate the values of the particles, which enables a computation process without a numerical mesh. Therefore, it is possible to model complex geometries and deal with large deformation (Das and Cleary, 2016). The Lagrangian formulation turns partial differential equations into ordinary differential equations which eliminate the non-linear convective terms and reduce numerical errors associated with the discretization of those terms. These features demonstrate the adaptability of SPH for various problems in different fields, which can be seen in recent developments of mesh-free and particle method (Liu and Liu, 2003a; Liu and Liu, 2003b; Shadloo et al., 2016).

Thus, the purpose of this present paper is to evaluate the applicability of the SPH method on heat conduction problems.

The study case is based on the unsteady heat conduction on a rectangular plate, which is a two-dimensional problem that has different temperatures on each side of the plate. This evaluation is made by a comparison among the numerical solution of the SPH method, the analytical solution and the numerical solution of the Finite Difference Method (FDM).

## 2. ANALYTICAL SOLUTION

The heat conduction on a rectangular plate is a two-dimensional problem modeled by the second-order parabolic PDE

$$\frac{\partial T}{\partial t} = \alpha \left( \frac{\partial^2 T}{\partial x^2} + \frac{\partial^2 T}{\partial y^2} \right), \tag{1}$$

where $\alpha$ is the thermal diffusivity of the plate material, $t$ is the time, $T$ is the temperature, $x$ and $y$ are vectors in the x-axis and y-axis, respectively. The steady-state of this problem can be solved by the Fourier analysis, also known as separable variables method. Thus, the temperature profile over a rectangular plate can be represented by

$$\begin{aligned} &T(x,y) = ... \\ &\sum_{n=1}^{\infty} \frac{2T_1\left[(-1)^{n+1}+1\right]}{n\pi \sinh\left(\frac{n\pi b}{a}\right)} \sin\left(\frac{n\pi x}{a}\right) \sinh\left(\frac{n\pi (y-b)}{a}\right) + \sum_{n=1}^{\infty} \frac{2T_2\left[(-1)^{n+1}+1\right]}{n\pi \sinh\left(\frac{n\pi a}{b}\right)} \sinh\left(\frac{n\pi x}{b}\right) \sin\left(\frac{n\pi y}{b}\right) + ... \\ &\sum_{n=1}^{\infty} \frac{2T_3\left[(-1)^{n+1}+1\right]}{n\pi \sinh\left(\frac{n\pi b}{a}\right)} \sin\left(\frac{n\pi x}{a}\right) \sinh\left(\frac{n\pi y}{a}\right) + \sum_{n=1}^{\infty} \frac{2T_4\left[(-1)^{n+1}+1\right]}{n\pi \sinh\left(\frac{n\pi a}{b}\right)} \sin\left(\frac{n\pi y}{b}\right) \sinh\left(\frac{n\pi (x-a)}{b}\right), \end{aligned} \tag{2}$$

where $T$ is the temperature profile, $T_i$, $i = 1, ..., 4$, are the boundary fixed temperatures at each side of the rectangular plate, Fig. 1, and $a$ and $b$ are the plate sides. Notably, the analytical solution depends only on the Dirichlet boundary condition rather than the plate material properties, leaving these parameters for the unsteady-state part like in the Couette flow between two infinite plates.

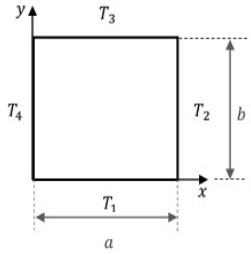


Figure 1. Rectangular plate diagram submitted to four different Dirichlet boundary conditions type.

Considering the phenomena as a linear one, it is possible to use the superposition principle such that

$$T(t,x,y) = T_s(x,y) + T_u(t,x,y), \tag{3}$$

where $T_s$ is the steady-state solution, Eq. (2), and $T_u$ is the unsteady-state part, on which is also applied the Fourier analysis to obtain a solution. It results in the double infinite series

$$T_u(t,x,y) = \sum_{m=1}^{\infty} \sum_{p=1}^{\infty} K_{mpn} \sin\left(\frac{m\pi x}{a}\right) \sin\left(\frac{p\pi y}{b}\right) \exp\left\{ -\left[ \left(\frac{m\pi}{a}\right)^2 + \left(\frac{p\pi}{b}\right)^2 \right] \alpha t \right\}, \tag{4}$$

where $K_{mpn}$ is a Fourier constant, which depends on $T_s$. Applying an appropriate integration and algebraic manipulation on $K_{mpn}$, it assumes the form of the infinite series

$$K_{mpn} = \sum_{n=1}^{\infty} \frac{8\left[(-1)^{n+1}+1\right]}{n\pi^2} \left( A_{mn}A_{pn} + B_{mn}B_{pn} + C_{mn}C_{pn} + D_{mn}D_{pn} \right), \tag{5}$$

where the variables $A_{mn}$, $A_{pn}$, $B_{mn}$, $B_{pn}$, $C_{mn}$, $C_{pn}$, $D_{mn}$, $D_{pn}$ are defined as

$$A_{mn} = C_{mn} = \begin{cases} \frac{a}{2} & \text{if } m = n \\ 0 & \text{if } m \neq n \end{cases}, \quad B_{pn} = D_{pn} = \begin{cases} \frac{b}{2} & \text{if } p = n \\ 0 & \text{if } p \neq n \end{cases}, \tag{6}$$

$$A_{pn} = -\frac{apT_1}{a^2p^2 + b^2n^2}, \quad B_{mn} = \frac{bmT_2(-1)^m}{a^2n^2 + b^2m^2}, \quad C_{pn} = \frac{bpT_3(-1)^m}{a^2p^2 + b^2n^2}, \quad D_{mn} = -\frac{amT_4}{a^2n^2 + b^2m^2}. \tag{7}$$

## 3. SPH METHOD

The representation of a function and its derivatives, in SPH, uses the integral convolution approximation, on which the particle approximation applies. Then, let $f$ be a continuous function over a domain $\Omega$ such that

$$f(\mathbf{x}) = \int_\Omega f(\mathbf{x}')\,\delta(\mathbf{x} - \mathbf{x}')\,\mathrm{d}\mathbf{x}' \approx \sum_{j=1}^{N} \frac{m_j}{\rho_j} f(\mathbf{x}_j)\,W(\mathbf{x} - \mathbf{x}_j, h), \tag{8}$$

where $\mathbf{x}$ is the position vector, $\delta(\mathbf{x} - \mathbf{x}')$ is the Dirac function, $m$ and $\rho$ are the mass and the density of the particles, respectively, $W(\mathbf{x} - \mathbf{x}_j, h)$ is the kernel function, which is the Dirac function approximation, $h$ is the smoothing length and $N$ is the total number of particles in the domain.

However, it is not enough to apply the SPH formulation without a well-defined kernel function, because it interpolates the contribution of each particle present in the compact domain. The kernel function should have the following properties to do it properly:

1. $\int_\Omega W(\mathbf{x} - \mathbf{x}', h)\,\mathrm{d}\mathbf{x}' = 1$;
2. $W(\mathbf{x} - \mathbf{x}_j, h) = 0$, for $|\mathbf{x} - \mathbf{x}_j| > \kappa h$;
3. $\lim_{h\to 0} W(\mathbf{x} - \mathbf{x}_j, h) = \delta(\mathbf{x} - \mathbf{x}_j, h)$.

The first property is the normalization one, which guarantees consistency for the integral representation. The second one is the Dirac function property, which allows the approximation $f(\mathbf{x}_i) \approx f(\mathbf{x})$. The last one is the compact support property, whose function is the transformation of a global process into a local one. Moreover, the kernel function should be positive, decreasing monotonous, symmetric, and sufficiently smooth. Figure 2 represents a kernel function with all these properties.

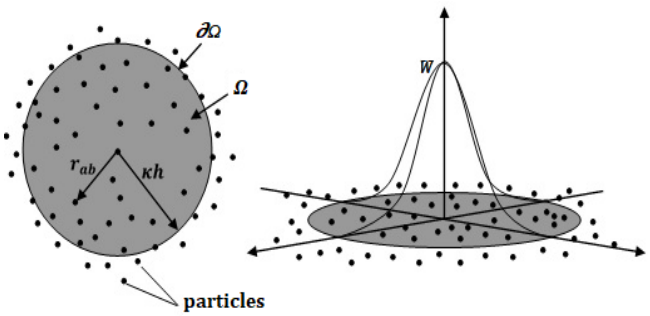


Figure 2. A schematic to demonstrate SPH interaction in compact domain

The kernel function used in this paper is the quartic spline defined as

$$W(s,h) = \alpha_h \begin{cases} \frac{2}{3} + \frac{9}{8}s^2 + \frac{19}{24}s^3 + \frac{5}{32}s^4, & s \leq 2 \\ 0, & s > 2 \end{cases} \tag{9}$$

where $s = (\mathbf{x} - \mathbf{x}_j)/h$ and $\alpha_h$ is $1/h$, $15/(7\pi h^2)$ and $315/(208\pi h^3)$ in one, two and three dimensions, respectively. The constant $\alpha_h$ is a consequence of the normalization property and as it can be observed in Eq. (9), the compact support is $2h$ ($\kappa = 2$). This kernel function is a proposed form of Liu and Liu (2003b), where it is shown the complete development of it, following all the properties cited above.

### 3.1 SPH approximation of the heat equation

The SPH method has a problematic second derivative formulation for most classical kernel functions because their second derivative is not a decreasing monotonous function, which implies several errors on the compact domain boundary. It is possible to apply a combined approximation using the SPH and the Taylor series to overcome this problem. So, the first step is to apply the SPH on the first derivative of the temperature such as

$$\nabla_i \left(k_i \nabla T_i\right) \approx \sum_{j=1}^{N} \frac{m_j}{\rho_j} \left(k_i \nabla T_i - k_j \nabla T_j\right) \nabla_j W_{ij}, \tag{10}$$

where $k$ is the thermal conductivity and $W_{ij} = W\left(\mathbf{x}_i - \mathbf{x}_j, h\right)$. The next step is to apply the Taylor series expansion on the first derivative terms in Eq. 10, which results in

$$\nabla_i \left(k_i \nabla T_i\right) \approx \sum_{j=1}^{N} \frac{m_j}{\rho_j} \left(k_i + k_j\right) \left(T_i - T_j\right) \frac{\nabla_j W_{ij}}{\mid \mathbf{x}_i - \mathbf{x}_j \mid}, \tag{11}$$

where

$$\frac{\nabla_j W_{ij}}{\mid \mathbf{x}_i - \mathbf{x}_j \mid} = \frac{1}{\mid \mathbf{x}_i - \mathbf{x}_j \mid} \frac{\mathbf{x}_i - \mathbf{x}_j}{\mid \mathbf{x}_i - \mathbf{x}_j \mid} \frac{\partial W_{ij}}{\partial \mid \mathbf{x}_i - \mathbf{x}_j \mid} = \frac{\mathbf{x}_{ij}}{r_{ij}^2} \frac{\partial W_{ij}}{\partial r_{ij}} \approx \frac{\mathbf{x}_{ij}}{r_{ij}^2 + \eta^2} \frac{\partial W_{ij}}{\partial r_{ij}} = F_{ij} \tag{12}$$

where $\mathbf{x}_{ij}$ is the relative distance vector between two particles, $r_{ij}$ is the norm of the relative distance vector, $\eta$ is a corrective constant whose value is $0.1h$.

Although this formulation is a good approximation for an isotropic material, it cannot deal with a non-isotropic one due to the presence of a discontinuity. Cleary and Monaghan (1999) developed a solution to improve the SPH method to overcome this problem. They approximated the temperature at the discontinuity, $T_d$, by the temperatures at the points $x_d \pm \Delta x/2$, assuming that the heat flow at these points is equal. Then, they expanded $T_d$ around $T_i$ and $T_j$, using a Taylor series. After that, these results were applied to Eq. 10, which yielded this new SPH formulation of the heat equation

$$\frac{DT_i}{Dt} \approx \frac{1}{\rho_i c_{v,i}} \sum_{j=1}^{N} \frac{m_j}{\rho_j} \left(\frac{4 k_i k_j}{k_i + k_j}\right) \left(T_i - T_j\right) F_{ij}, \tag{13}$$

where $c_v$ is the specific heat.

### 3.2 Particle mass

The mass definition for each particle influences the time convergence of the method. This happens due to the directly proportional relationship between the mass and the volume, considering the density as a constant. As a result, if the mass increases, then the particle volume size also increases, which means that the distance between one particle's surface to other decreases. Therefore, the amount of time of one particle to cover this distance and hit other particles decreases, reflecting on the rate of the thermal energy transfer. In other words, the time to reach the steady-state is inversely proportional to mass.

Furthermore, it is not simple to define a three-dimensional concept, like volume, from a two-dimensional problem, keeping the physical meaning, because there is not a third dimension available. Thus, the numerical total volume can be defined as $V = ab\xi$, where $a$ is the plate's length, $b$ is the plate's width and $\xi$ is a constant, which substitutes the plate's height and helps to adjust the mass, in order to find its proper value. Therefore, the definition of each particle mass is

$$m_i = \frac{\rho V}{N} = \frac{\rho a b \xi}{N}. \tag{14}$$

### 3.3 Time integration

It was used the second-order Runge-Kutta method, also known as the improved Euler method, to integrate Eq. (13) in time, which gives an error of order $O\left(\Delta t^2\right)$. The numerical formulation of this method for a continuous function $f$ is

$$k1 = g\left(t^n, f^n\right),$$
$$k2 = g\left(t^n + \frac{\Delta t}{2}, f^n + \frac{\Delta t}{2} k_1\right),$$
$$f^{n+1} = f^n + \Delta t\, k_2.$$

The size of the time step for a pure conduction problem is given by

$$\Delta t = \frac{\beta \rho c_v h^2}{k}, \tag{15}$$

where $\beta$ is a constant, whose value is limited by stability, $h = 1.2\Delta x$ and $\Delta x$ is the particle spacing.

## 4. FINITE DIFFERENCE METHOD

In this section, a classical Finite Difference Method is presented: the forward time central space (FTCS) Euler scheme. This method has an error of order $O\left(\Delta t^2, \Delta x^2, \Delta y^2\right)$ and is a direct approach to discretize the heat equation. The discretization takes the form

$$T_{i,j}^{n+1} = T_{i,j}^n + \frac{k}{\rho c_v}\frac{\Delta t}{\Delta x^2}\left[T_{i+1,j}^n - 2T_{i,j}^n + T_{i-1,j}^n\right] + \frac{k}{\rho c_p}\frac{\Delta t}{\Delta y^2}\left[T_{i,j+1}^n - 2T_{i,j}^n + T_{i,j-1}^n\right]. \tag{16}$$

The numerical stability criteria is given by

$$\Delta t = \frac{\gamma \rho c_v}{k}\left(\Delta x^2 + \Delta y^2\right), \tag{17}$$

where $\gamma$ is the Courant-Friedrich-Lewy constant (Courant et al., 1928), and it must be less or equal than a quarter.

## 5. BOUNDARY CONDITIONS

Similar approaches were used to implement the boundary conditions for both numerical methods. Two layers of fixed ghost particles form the boundary for the SPH method, Fig. 3. While, two layers of ghost mesh compose the boundary of FDM, which behaves similarly to the ghost particles.

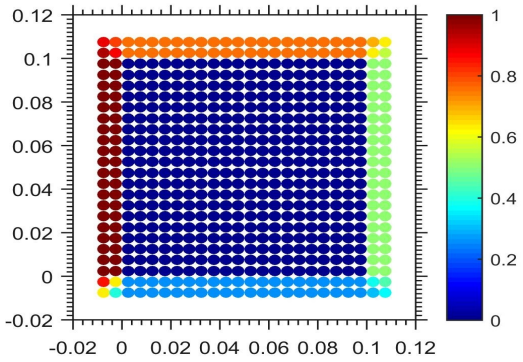


Figure 3. Distribution of the initial temperature and the boundary conditions over the real and ghost particles.

In Fig. 3, the dark blue dots represent the real particles at the initial state of the plate, which, in this paper, is $T(0, x, y) = 0\,^oC$. The other dots, which are distributed in two layers outside the dark blue ones, are the ghost particles, whose temperature remains unchanged during the computation process. However, the ghost particles integrate the compact domain of the real particles next to the boundaries, Fig. 4. Therefore, their influence acts on the real particles through the kernel function. A similar process occurs in the FDM

## 6. RESULTS

In order to evaluate the applicability of SPH on the heat conduction problem, a plain carbon steel plate with $10 \times 10\ cm$ dimensions, $\rho = 7854\ kg/m^3$, $c_v = 0.434\ kJ/kgK$, $k = 60.5\ W/mK$, was chosen (Bergman et al., 2002). The

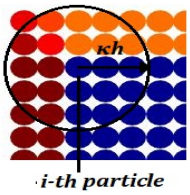


Figure 4. Particles in the compact domain of a i-th particle, including itself.

boundary conditions were set as $T_1 = 0.25\ ^oC$, $T_2 = 0.50\ ^oC$, $T_3 = 0.75\ ^oC$ and $T_4 = 1.00\ ^oC$ and the initial condition was $T\,(0, x, y, ) = 0\ ^oC$. In SPH, 400 real particles and 176 ghost particles were used, the particles center distance were $\Delta x = \Delta y = 0.005\ m$, the smoothing length was $h = 1.2\Delta x$ and $\xi = 1.643\ m$, which means that $m_i = 0.224\ kg$. For FTCS Euler schemes, $\Delta x = \Delta y = 0.005\ m$ were used , which states the same resolution for both two numerical methods. In FTCS Euler scheme, $\gamma = 0.029$ was set . The models were run using an Intel Core i5-3337U CPU (1.8 GHz) with 4 GB RAM on a Windows 10 operating system. Additionally, the codes were compiled using Matlab R2015a.

The SPH solution result, the red isothermal contours, was compared with the analytical solution, the black isothermal contours, in Fig. 5, which is divided into the instants $t = 28.8894\ s$, $t = 57.9411\ s$, $t = 86.9928\ s$ and $t = 115.8822\ s$. The temperatures near the left and the top sides of the plate are relatively high in the first instants, but they drop along the time due to the transport energy effect. When the steady-state is reached, at $t = 115.8822s$, a clear division between the hot region and the cold one is observed through a diagonal line, which is a middle value among the boundaries temperatures. The SPH solution follows the analytical solution with an accuracy of order $10^{-2}$.

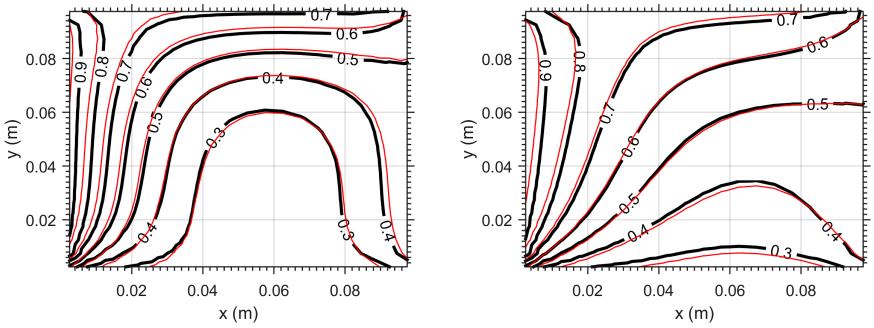


(a) Isothermal contours for t = 28.8894 s

(b) Isothermal contours for t = 57.9411 s

(c) Isothermal contours for t = 86.9928 s

(d) Isothermal contours for t = 115.8822 s

Figure 5. Comparison between the analytical and the SPH solutions. The analytical isothermal contours are the black ones, while the SPH isothermal contours are red.

In Fig. 6, a similar comparison is made between the FTCS Euler scheme, and the analytical solution, where the black isothermal contours represent the analytical solution and the red ones represent the numerical solution. The FTCS Euler result has almost the same accuracy as the SPH result, Tab. 1 and both methods show a decreasing error along the time. However, FTCS Euler presents 776 times less computational cost, which shows that SPH has competitive accuracy, but it needs to improve its computational cost.

Moreover, the maximum error is higher near the edges and the boundaries of the plate. Considering the time frame of $28.8894\ s$, the maximum error near the left boundary is around $5\%$, while the error at the center of the plate is around $2\%$. These are the consequences of the particle deficiency near or on the boundaries that are caused by truncation of the integral and is known as the edge effect. As a result, the heat transfer along the edges and boundaries becomes slower

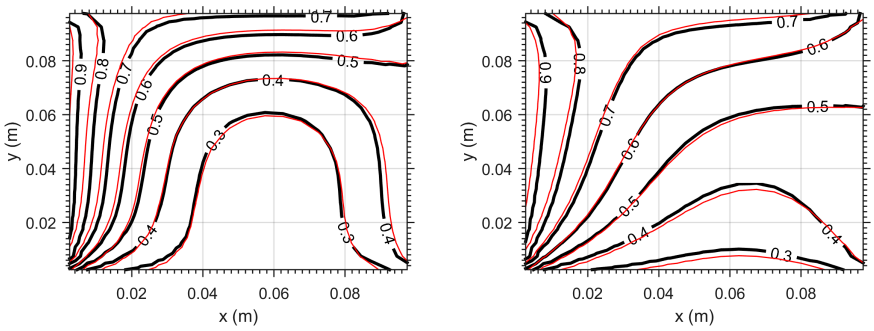


(a) Isothermal contours for t = 28.8894 s

(b) Isothermal contours for t = 57.9411 s

(c) Isothermal contours for t = 86.9928 s

(d) Isothermal contours for t = 115.8822 s

Figure 6. Comparison between the analytical and the FTCS Euler scheme solutions. The analytical isothermal contours are the black ones, while the FTCS Euler isothermal contours are red.

Table 1. Comparison between the two numerical methods used to model the heat conduction on a rectangular plate.

| | Average Error $(\%)$ | | | | |
|---|---|---|---|---|---|
| Method | $t = 28.8894\ s$ | $t = 57.9411\ s$ | $t = 86.9928\ s$ | $t = 115.8822\ s$ | Computational Cost $(s)$ |
| SPH | 2.7827 | 2.0474 | 1.9732 | 1.9661 | 1242.2 |
| FTCS Euler | 2.6552 | 2.0476 | 1.9619 | 1.9412 | 1.6 |

than through the center of the plate. The mass of the particles influences the edge effect, which increases or decreases the heat transfer, especially near the boundaries. Therefore, one way to reduce this effect is through the proper choice of $\xi$, the numerical parameter which acts as the material height. So, we made an investigation about this parameter, considering relative average error as a criterion to define a value of $\xi$ as a proper one. Furthermore, to reduce bias in this investigation, we used three different materials properties: plain carbon steel, titanium, and vanadium. We cited the first material properties above. The titanium properties are $\rho = 4500\ kg/m^3$, $c_v = 0.522\ kJ/kgK$, $k = 21.9\ W/mK$, while the vanadium properties are $\rho = 6100\ kg/m^3$, $c_v = 0.489\ kJ/kgK$, $k = 30.7\ W/mK$ (Bergman et al., 2002). Besides, the considered time frame was $t = 28.8894\ s$ because it has higher errors compared with the other presented time frames and has the least computation time. Figure 7 presents the results of this investigation.

In Fig. 7 (b) a directly proportional relationship between the smoothed length and $\xi$ can be pointed. To explain this fact, let to consider $\xi$ constant and decrease the value of $h$. This consideration raises the number of particles with the same volume inside the same total volume, which, as a consequence, enlarges the surface contact. Thus, the heat transfer is intensified, advancing more quickly in time than the analytical solution. As a result, it is necessary to reduce the volume of the particles to slow down the numerical solution. A similar process occurs with the increasing of $h$. Furthermore, the curves in Fig. 7 (b) behave similarly with a maximum standard deviation of $0.0302\ m$. There is not a specific equation capable of perfectly modeling $\xi\,(h)$ as a function of only $h$ because the material properties have also some influence, which produces the deviations presented in Fig. 7 (b). But, the potential form

$$\xi\,(h) \approx 9h^{1/3}, \tag{18}$$

provides a suitable initial value for $\xi$, considering $h \leq 0.007\ m$. The rise of error in assuming Eq. (18) is around $3.5\%$.

The error curves in Fig. 7 (a) assume similarly behave, which shows a concordance independently of the material properties. The SPH method has a first space global order error (Liu and Liu,2003a) and the observed order is verified

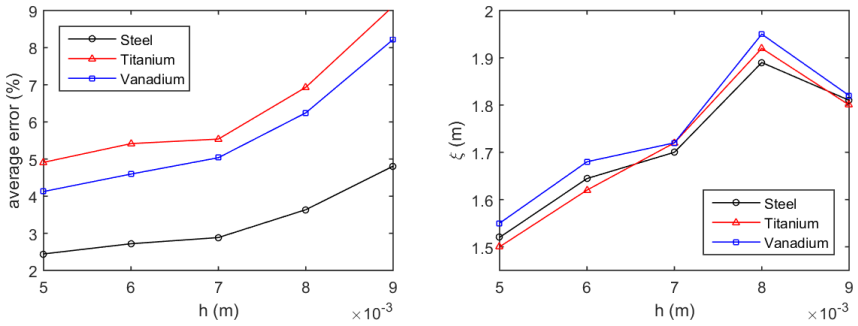


(a) (b)

Figure 7. At left, the minimum errors associated to $\xi$ are presented in function of the smoothed length, while, at right, it is placed the evolution of $\xi$ relatively to $h$.

with (Roache, 1998)

$$p \approx \frac{\log\left(\frac{E_2}{E_1}\right)}{\log r}, \tag{19}$$

where $E_1$ and $E_2$ are error for the coarse and fine resolution, respectively, and $r = h_2/h_1$ is the refinement factor between the coarse and fine resolutions. So, considering $h_1 = 0.009\ m$ and $h_2 = 0.005\ m$, the average observed order of accuracy is $p = 1.1253$, which agrees with the expected order value. Moreover, the divergence among the error curves is caused by the time step change, Eq. 15, because it depends on the material properties such that $\Delta t_{titanium} > \Delta t_{vanadium} > \Delta t_{steel}$.

Another aspect of the SPH method is computational cost. It has a higher one due to the number of internal summations, which are executed in serial order of computation in the CPU. The effect of this is an exponential increase in the processing time when the number of particles rises, Fig. 8. The divergence present among the materials is related to the step time because a change in it affects the number of iterations necessary to reach some set time.

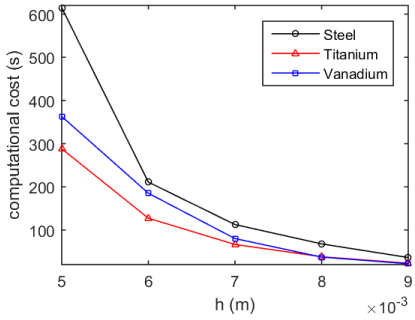


Figure 8. Computational cost for the numerical solution at $t = 28.8894\ s$. It has an exponential behave in function of the smoothed length.

## 7. CONCLUSION

Results using the SPH method present global order convergence of 1.1253, which agrees with theoretical value and with the FCTS Euler finite difference method. As a result, the error decays along time, which shows that SPH is a capable technique for modeling unsteady-state thermal conduction at several frames of time. Both two numerical methods show edge and boundary effects, which lowers the heat transfer and causes a decreasing in the accuracy near these regions. However, to guarantee the convergence order and reduce the boundaries effects, it is necessary to select a proper value for $\xi$, which turned out to have a simple relation with the smoothed length. Although SPH presents excellent results and agreement with the analytical solution, there is a problem with the computational cost, which can be reduced with the code parallelization.

## 8. REFERENCES

Beck, J. V., Blackwell, B. and St. Calir, C. R.,jr., 1987. "Inverse heat conduction: ill-posed problems". *ZAMM - Journal of Applied Mathematics and Mechanics / Zeitschrift Für Angewandte Mathematik Und Mechanik*, Vol. 67, No. 3, pp. 212–213.

Bergman, L. T., Lavine, S. A., Incropera, F. P. and Dewitt, D. P., 2002. *Fundamentals of heat and mass transfer*. John Wiley & Sons Inc., United States of America, 7th edition.

Ceretani, A. N., Tarzia, D. A., and Villa, L. T., 2015. "Explicit solutions for a non-classical heat conduction problem for a semi-infinite strip with a non-uniform heat source. Boundary Value Problems". *Springer Open Journal*, Vol. 156, pp. 1–26.

Chiba, R., 2018 "An analytical solution for transient heat conduction in a composite slab with time-dependent heat transfer coefficient". *Mathematical Problems in Engineering*, Vol. 2018, pp. 1–11.

Cleary, P. W. and Monaghan, J. J., 1999. "Conduction modelling using smoothed particle hydrodynamics". *Journal of Computational Physics*, Vol. 144, pp. 227–264.

Das, R., and Cleary, P. W., 2016. "Three-dimensional modelling of coupled flow dynamics, heat transfer and residual stress generation in arc welding processes using the mesh-free SPH method". *Journal of Computational Science*, Vol. 16, pp. 200–216.

Deconinck, B., Pelloni, B., and Sheils, N. E., 2014. "Non-steady-state heat conduction in composite walls". *Proceedings of the Royal Society A: Mathematical, Physical and Engineering Sciences*, Vol. 470, pp. 1–22.

Courant, R., Friedriches, K. and Lewy, H., 1928. "Über die partiallen Differenzengleichungen der mathematischen Physik". *Mathematische Annalen*, Vol. 100, pp. 32–74.

Gingold, R. A. and Monaghan, J. J., 1977. "Smoothed particle hydrodynamics:theory application to non-spherical stars". *Monthly Notices of the Royal Astronomical Society*, Vol. 181, No. 3, pp. 375—389.

Kudinov, I. V., Kudinov, V. A. and Kotova, E. V., 2017. "Additional boundary conditions in unsteady-state: heat conduction problems". *Teplofizika Vysokikh Temperatur*, Vol. 55, No. 4 pp. 556–563.

Liu, G. R. and Liu, M. B., 2003a. *Mesh-Free methods: moving beyond the finite element method*. CRC Press, New York, 1st edition.

Liu, G. R. and Liu, M. B., 2003b. *Smoothed particle hydrodynamics: a meshfree particle method*. World Scientific Publishing Co. Pte. Ltd., Singapore, 1st Edition.

Lucy, L. B., 1997. "A numerical approach to the testing of fusion process". *Astronomical Journal*, Vol. 88, No. 12, pp. 1013—1024.

Mavropoulos, G. C., 2011. "Unsteady heat conduction phenomena in internal combustion engine chamber and exhaust manifold surfaces". *Heat Transfer - Engineering Applications*, Vol. 2011, pp. 283–308.

Myint-U, T. and Debnath, L., 2007. *Linear differential equations for scientists and engineers*. Birkhäuser, Boston, 4th edition.

Peng, Y., Zhu, Z. and Chen, G., 2011. "Heat conduction for helical and periodical contact in a mine hoist". *Heat Transfer - Engineering Applications*, Vol. 2011, pp. 231–258.

Roache, P. J., 1998. "Verification of codes and calculations.". *American Institute of Aeronautics and Astronautics (AIAA) Journal*, Vol. 36, No. 5, pp. 696–702.

Shadloo, M. S., Oger, G. and Le Touze, D., 2016. "Smoothed particle hydrodynamics method for fluid flows, toward industrial applications: motivations,current state,and challenges". *Computer and Fluids*, Vol. 136, pp. 11–34.

Tanana, V. P. and Sidikova, A. L., 2018. *Optimal methods for ill-posed problems: with applications to heat conduction*. de Gruyter, Inverse and Ill-Posed Problems Series (62), 1st edition.

Zima, W., 2011. "Mathematical modelling of dynamics of boiler surfaces heated convectively". *Heat Transfer - Engineering Applications*, Vol. 2011, pp. 259–282.

## 9. RESPONSIBILITY NOTICE

The authors are the only responsible for the printed material included in this paper.